Positioning particles within liquids using ultrasound force fields

PACS REFERENCE: 43.20.Ks, 43.25.Qp, 43.25.Uv

Hawkes Jeremy J.[1], Gröschl Martin [2], Benes Ewald [2], Nowotny Helmut [3], Coakley W. Terence [4]

[1] Department of Instrumentation and Analytical Science
University of Manchester, Institute of Technology
PO Box 88, Manchester M60 1QD, UK
Email: j.hawkes@umist.ac.uk

[2] Vienna University of Technology, Institut für Allgemeine Physik
Wiedner Hauptstr. 8-10/134, A 1040 Wien
Email: groeschl@iap.tuwien.ac.at, benes@iap.tuwien.ac.at

[3] Vienna University of Technology, Institut für Theoretische Physik
Wiedner Hauptstr. 8-10/136, A 1040 Wien
Email: hnowotny@pop.tuwien.ac.at

[4] School of Biosciences, Cardiff University
Cardiff CF10 3TL, UK
Email: coakley@cf.ac.uk

ABSTRACT

Ultrasound standing wave radiation acts on suspensions, emulsions, and colloids to drive the dispersed particles (solid particles, bubbles, or oil droplets) towards either nodal or anti-nodal positions in the sound field. Using narrow chambers which contain only one nodal plane we have been able to position this pressure node at: 1) The reflector side wall of a chamber, this has been used to draw cells to a surface for detection by a biosensor. 2) The centre of the chamber, this has been combined with manipulation by laminar flow to produce a filter to remove contaminating particles. These systems have been developed using a one-dimensional transfer matrix model to predict the node positions and the acoustic energy density in the fluid. The model has been further used to predict chamber designs in which pressure nodes are at 1) the transducer side wall of the chamber and 2) both walls of the chamber.

INTRODUCTION

When an ultrasound standing wave is created in a suspension of particles a force is exerted on the particles either towards the pressure nodes or the antinodes. For example, bacteria in an aqueous suspension move towards the pressure nodes. This is because the mass density and the speed of sound in the cells are greater than the respective values of the medium. In contrast, oil droplets or air bubbles dispersed in water move towards the pressure antinodes, because their density and speed of sound are lower than for the medium. The magnitude and direction of these acoustic radiation forces have been discussed elsewhere (King, 1934; Yosioka and Kawasima, 1955; Gor'kov, 1962; Nyborg, 1967; Crum, 1971; Gould and Coakley, 1974; Whitworth and Coakley, 1992; Gröschl, 1998). The subject of this paper is the position of nodes within the chamber itself. This is of particular importance for the development of short pathlength chambers that contain a single node (Johnson and Feke, 1995; Hawkes and Coakley, 2001; Hawkes et al., 2002). The Reynolds number is very low for such short pathlength chambers (e.g. 11 for a 0.25 mm chamber with an average flow velocity of 60 mm/s) with laminar flow conditions throughout the chamber. Two applications for these systems currently under development are: 1) a particle filter consisting of a chamber with a region of standing wave radiation where particles are moved to a central nodal position, followed by a region which takes advantage of the laminar flow where the clear medium on either side of the central particles is drawn away (Hawkes et al., 2002; Hawkes and Coakley, 2001); 2) a system

to enhance the particle capture rate of biosensor surfaces by driving particles to the wall of the chamber (unpublished).

The aim of this paper is to describe fundamental design criteria, which must be applied for the development of any ultrasound system where node positioning is required. Four positions where the node can be placed between two chamber walls will be considered, these are against the transducer wall, centrally between the walls, against the reflector wall and against both walls. The method for calculating the node positions is based on the transfer matrix multilayer model. The reliability of this model was tested previously (Hawkes et al., 2002), here it is used as a design tool.

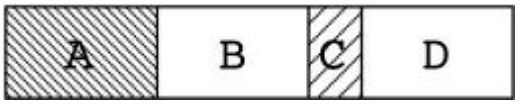

Fig. 1 Schematic representation of the acoustic chamber (4-layer system): A piezoceramic, B stainless steel transmission layer, C water layer, D stainless steel reflector layer.

Table 1 Material properties

	Piezoceramic A	Steel B, D	Water C
Speed of sound [m/s]	4080	6100	1500
Mass density [kg/m^3]	7700	7800	1000
Acoustic quality factor	1000	1000	1000
Dielectric constant [F/m]	1.2 x 10^{-8}		
Tangent of dielectric loss angle	3.0 x 10^{-3}		
Electromechanical coupling factor	0.48		
Electrode area [mm^2]	200		
Thickness Q = λ/4 (@ 3 MHz) [mm]		0.508	0.125
Thickness H = λ/2 (@ 3 MHz) [mm]	0.680	1.016	0.250

SIMULATION CHOICES

A model (Nowotny and Benes, 1987; Nowotny et al., 1991) to simulate acoustic wave propagation through a multilayer system is used. This transfer matrix multilayer model has recently been experimentally validated in detail (Hawkes et al., 2002; Gröschl, 1998). Here the model has been run using data and construction details similar to those used for the experimental verification (Hawkes et al., 2002), see Figure 1. The ultrasound is produced by a piezoceramic layer (A), transmitted to the water layer (C) through stainless steel (B) and reflected by a second layer of stainless steel (D). The relevant properties of these layers are given in Table 1. The aim here is to describe general design principles. For this purpose we choose a fundamental frequency of 3 MHz and acoustic quality factors of 1000 for the different layers (previous fitted quality factor results were 150 and 350 for water and the piezoceramic respectively, while data for pure water is more than 10,000 and manufacturer data for the piezoceramic is 1000). Furthermore, the glue layer to fix the ceramic to the transmission layer is not considered here. The thicknesses of the transmission and reflector layers are modelled with values which at 3 MHz are exactly λ/2, λ/4 and 0 and for water λ/2 and λ/4. The corresponding dimensions in mm are given in the last two rows of Table 1. These λ/4 steps represent the extremes for the node positions. Results will be very similar for systems with thicker layers. For example, a λ/4 layer will behave in a similar manner to 3λ/4, 5λ/4 etc layers, and a λ/2 layer will behave in a similar manner to λ, 3λ/2 etc layers. Increasing the number of wavelengths in a system will alter frequency spectra bringing the peaks closer together.

Construction codes

The large numbers of constructions considered here are referred by the thickness values of the component layers in terms of wavelength at 3 MHz: 0 = no layer, Q = λ/4, H = λ/2. The piezoceramic layer is modelled with constant thickness of λ/2 and is not included in the code. The passive layers are described by three letters, 0HQ for example refers to a construction with no transmission layer, λ/2 water layer (0.25 mm) and λ/4 stainless steel reflector (0.508 mm).

SIMULATION RESULTS AND DISCUSSION

In Figures 2a and 2b the spatial distributions of the pressure and the acoustic energy density along the sound path (thickness direction of the layers) are shown for all considered constructions (all combinations of transmission layer and reflector thicknesses with λ/4 and λ/2 water layer thicknesses, respectively). For these calculations it was assumed that the electrodes of the piezoceramic are connected to an electric generator with a source voltage amplitude of 1 V and a source resistance of 50 Ω. Since on the free outer surface of the reflector there is always a pressure node, for all constructions xy0 and xyH (x and y are any codes for the transmission layer and the reflector layer thickness, respectively) there is also a pressure node at the right boundary of the water layer. For a water layer thickness of λ/2 (codes xH0 and xHH) there is an additional pressure node at the other boundary (interface between layers B and C). A pressure node in the middle of the water layer can only occur for a λ/2 water layer combined with a λ/4 reflector layer (code xHQ). As can be seen from the pressure scales, high values of pressure are obtained particularly in cases where the total acoustic path length is a multiple of λ/2 (these are 0QQ, QQ0, QQH, HQQ in Fig. 2a and 0H0, 0HH, QHQ, HH0, HHH in Fig. 2b).

The acoustic energy density in the water layer is also dependent on the reflector thickness. For a reflector thickness of λ/2 (codes xyH), the acoustic energy density is much higher in the reflector than in the adjacent water layer, because for these geometries the displacement amplitudes have the same maximum value in both layers. This follows from the condition of continuity for the displacement that must apply at the water-reflector interface. In Figs. 3a and 3b the frequency spectra of the acoustic energy density in the water layer for all considered constructions are shown. As for Fig. 2, a source voltage amplitude of 1 V and a source resistance of 50 Ω were assumed. Since the electric impedance of the multilayer systems is strongly dependent on frequency, the voltage at the piezoceramic, as well as the total electric input energy to the system, also vary with frequency. Therefore, these figures alone are not sufficient to predict the efficiency of a particular construction. For the piezoceramic's resonance frequency of 3 MHz, the acoustic energy density in the water layer shows maxima for all designs with a total acoustic path length that equals a multiple of λ/2 at 3 MHz (0QQ, QQ0, QQH, HQQ in Fig. 3a, 0H0, QHQ, HH0 in Fig. 3b). Although this condition is not fulfilled for the designs 0QH and HQH (Fig. 3a), the results look very similar to the spectra for 0QQ and HQQ, respectively. However, this similarity is not a basic property of these designs but is due to a smoothing effect on the energy density spectra that is caused by the 50 Ω source resistance in series with the piezoelectric structure. To illustrate this effect, in the upper right picture of Fig. 3a (design 0QH) the respective energy density spectrum for a zero source resistance is included (blue curve). This curve shows a double peak, which is characteristic for designs where the total acoustic path length at 3 MHz does *not* match a multiple of λ/2.

Other designs that do not fulfill the wavelength criterion can be identified in Figs. 3a and 3b. These designs either show a double peak near 3 MHz (0Q0, HQ0, 0HQ, QHH, HHQ) or peaks far below and above 3 MHz but not near the piezoceramic's fundamental (QQQ, QH0). Finally, the designs 0HH and HHH (Fig. 3b) show only very small maxima at 3 MHz, surrounded by two greater peaks below and above 3 MHz, respectively, although they fulfil the wavelength criterion at 3 MHz. However, the peak at 3 MHz is smoothed out due to the effect of the driving source resistance, which at 3 MHz is large compared to the resonator impedance.

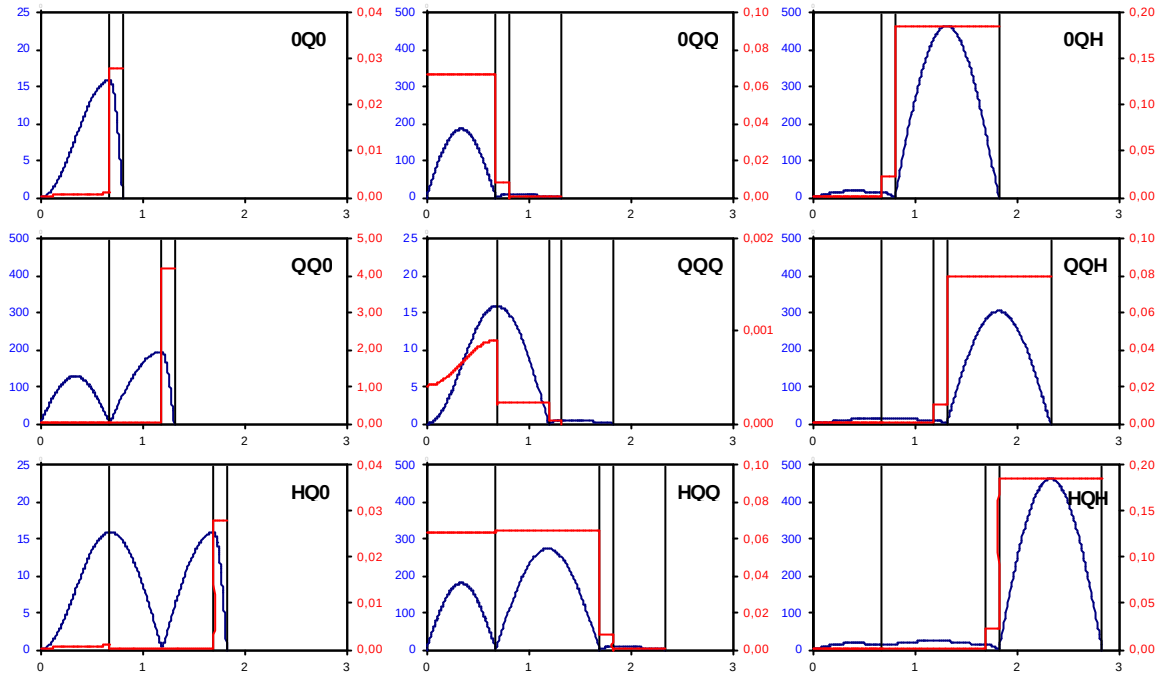

Fig. 2a Distributions of pressure (scale in kPa on the left) and acoustic energy density (scale in J/m^3 on the right) along the sound path at 3 MHz for all 9 possible constructions for a chamber with a water layer of λ/4 (0.125 mm) and 0, λ/4 or λ/2 stainless steel transmission and reflector layers. Pressure drops to 0 at the node positions. Layer boundaries are indicated by black vertical lines. Results are valid for an electric drive generator with a source voltage amplitude of 1 V and a source resistance of 50 Ω. Scale on the horizontal axis (sound path) is given in mm.

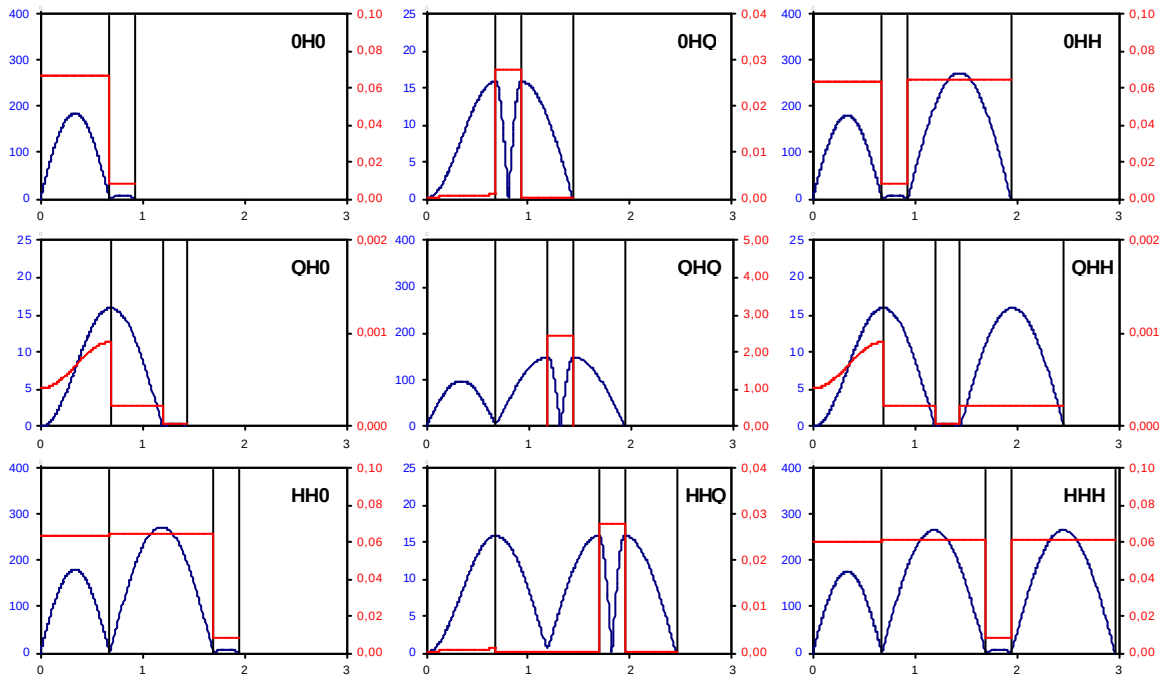

Fig. 2b The same as Fig. 2a but with a water layer of λ/2 (0.25 mm) and 0, λ/4 or λ/2 stainless steel transmission and reflector layers.

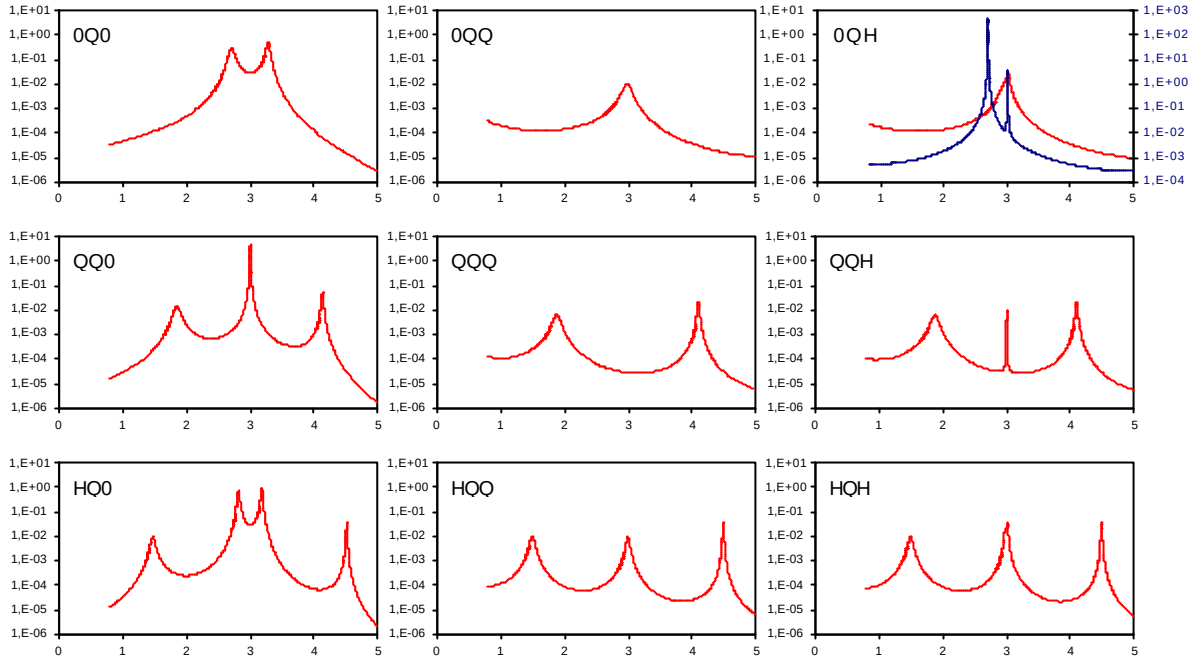

Fig. 3a Frequency spectra of the acoustic energy density (in J/m^3) within the water layer for all 9 possible chambers with a water layer of λ/4 (0.125 mm) and 0, λ/4 or λ/2 stainless steel transmission and reflector layers (the thickness values given in fractions of the acoustic wavelength correspond to a frequency of 3 MHz). Results are valid for an electric drive generator with a source voltage amplitude of 1 V and a source resistance of 50 Ω. The upper right picture additionally shows the result for a zero source resistance (blue curve, scale on the right). Scale on the horizontal axis (frequency) is given in MHz.

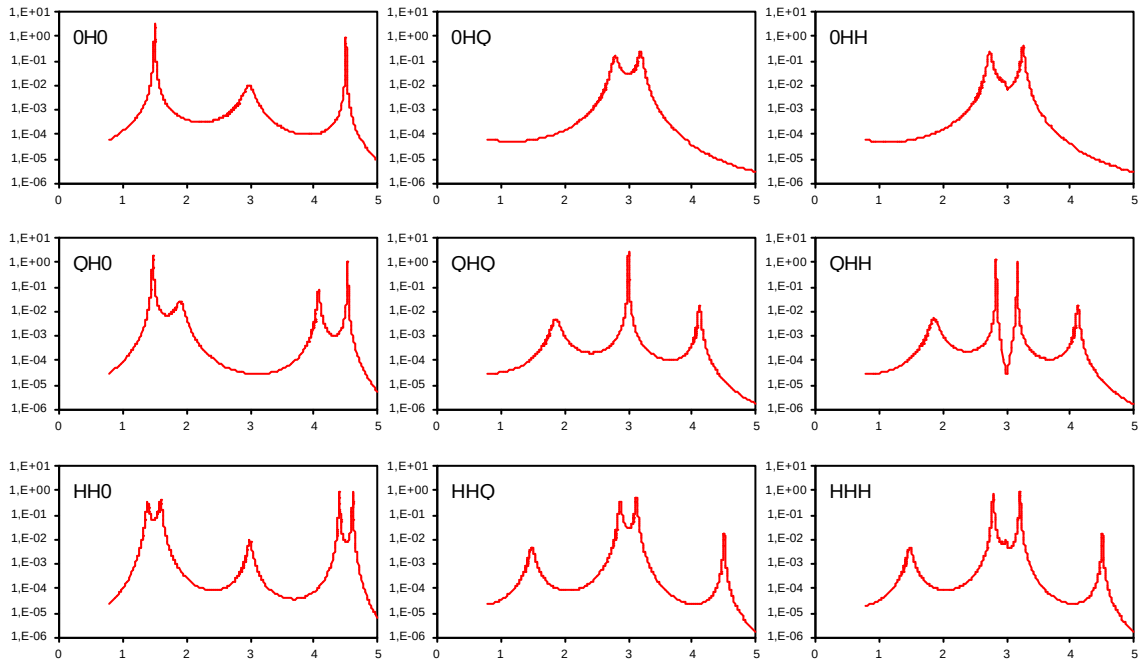

Fig. 3b The same as Fig. 3a but with a water layer of λ/2 (0.25 mm) and 0, λ/4 or λ/2 stainless steel transmission and reflector layers.

Similar results for node positions and spectra have been obtained, although with altered peak magnitudes, when carbon (speed of sound 4260 m/s, mass density 1470 kg/m^3) or silicon (speed of sound 8430 m/s, mass density 2340 kg/m^3) was used in the simulations.

CONCLUSION

The discussed series of designs describe constructions, which can be chosen to position particles either at a wall or centrally within a chamber. Moving particles from the centre of a chamber to the chamber walls is also possible by a change in frequency. In particular, this can be achieved in chambers 0HH or HHH. Particles may be also moved from one wall to the other. With respect to system efficiency, it is advantageous to operate near the piezoceramic's fundamental resonance. Nonetheless, other operating frequencies may produce some useful systems.

ACKNOWLEDGEMENTS

Jeremy J. Hawkes was supported by a DERA Contract No. CU013-0000010785. Work supported by the European Commission's TMR Programme EuroUltraSonoSep, Contract No. ERBFMRXCT97-0156, .

REFERENCES

Crum, L.A. Acoustic force on a liquid droplet in an acoustic stationary wave, J. Acoust. Soc. Am. 50, 157-163 (1971).

Gor'kov, L.P. On the forces acting on a small particle in an acoustical field in an ideal fluid, Sov. Phys. Dokl. 6, 773-775 (1962).

Gould, R.K., and Coakley, W.T. The effects of acoustic forces on small particles in suspension, Proc. 1973 Symp. on Finite-Amplitude Wave Effects in Fluids (Pergamon Press, Guildford, UK, 1974), pp. 252-257.

Gröschl, M. Ultrasonic separation of suspended particles - Part I: Fundamentals, Acustica - acta acustica 84, 432-447 (1998).

Hawkes, J.J., and Coakley, W.T. Force field particle filter, combining ultrasound standing waves and laminar flow, Sensors and Actuators B 75, 213-222 (2001).

Hawkes, J.J., Coakley, W.T., Gröschl, M., Benes, E., Armstrong, S., Tasker, P.J., and Nowotny, H. Single half-wavelength ultrasonic particle filter: Predictions of the transfer matrix multilayer resonator model and experimental filtration results, J. Acoust. Soc. Am 111, 1259-1266 (2002).

Hill, M., Harris, N.R., Townsend, R., Beeby, S.P., Shen, Y., White, N.M., Hawkes J.J., and Coakley, W.T. A microfluidic device for ultrasonic separation, Proc. Forum Acusticum 2002, Sevilla, Spain, Sept. 16-20, 2002.

Johnson, D.A., and Feke, D.L. Methodology for fractionating suspended particles using ultrasonic standing wave and divided flow fields, Separations Technology 5, 251-258 (1995).

King,, L.V. On the acoustic radiation pressure on spheres, Proc. R. Soc. London A147, 212-240 (1934).

Nowotny, H., and Benes, E. General one-dimensional treatment of the layered piezoelectric resonator with two electrodes, J. Acoust. Soc. Am. 82, 513-521 (1987).

Nowotny, H., Benes, E., and Schmid, M. Layered piezoelectric resonators with an arbitrary number of electrodes (general one-dimensional treatment), J. Acoust. Soc. Am. 90, 1238-1245 (1991).

Nyborg, W.L. Radiation pressure on a small rigid sphere, J. Acoust. Soc. Am. 42, 947-952 (1967).

Whitworth, G., and Coakley, W.T. Particle column formation in a stationary ultrasonic field, J. Acoust. Soc. Am. 91, 79-85 (1992).

Yosioka, K., and Kawasima, Y. Acoustic radiation pressure on a compressible sphere, Acustica 5,167-173 (1955).